Absolute elastic differential cross sections for electron scattering by $C_6H_5CH_3$ and $C_6H_5CF_3$ at 1.5–200 eV: A comparative experimental and theoretical study with C_6H_6

H. Kato, M. C. Garcia,* T. Asahina, M. Hoshino,† C. Makochekanwa,‡ and H. Tanaka
Department of Physics, Sophia University, 7-1 Kioicho, Chiyoda-ku, Tokyo 102-8554, Japan

F. Blanco
Departamento de Física Atómica, Molecular y Nuclear, Universidad Complutense de Madrid, Avenida Complutense s.n., 28040 Madrid, Spain

G. García
Instituto de Matemáticas y Física Fundamental, Consejo Superior de Investigaciones Científicas, Serrano 121, 28006 Madrid, Spain
(Received 20 December 2008; published 4 June 2009)

We present absolute differential cross sections (DCS) for elastic scattering from two benzene derivatives $C_6H_5CH_3$ and $C_6H_5CF_3$. The crossed-beam method was used in conjunction with the relative flow technique using helium as the reference gas to obtain absolute values. Measurements were carried out for scattering angles 15°–130° and impact energies 1.5–200 eV. DCS results for these two molecules were compared to those of C_6H_6 from our previous study. We found that (1) these three molecules have DCS with very similar magnitudes and shapes over the energy range 1.5–200 eV, although DCS for $C_6H_5CF_3$ increase steeply toward lower scattering angles due to the dipole moment induced long-range interaction at 1.5 and 4.5 eV, and (2) that the molecular structure of the benzene ring significantly determines the collision dynamics. From the measured DCS, elastic integral cross sections have been calculated. Furthermore, by employing a corrected form of the independent-atom method known as the screen corrected additive rule, DCS calculations have been carried out without any empirical parameter fittings, i.e., in an *ab initio* nature. Results show that the calculated DCS are in excellent agreement with the experimental values at 50, 100, and 200 eV.

DOI: 10.1103/PhysRevA.79.062703 PACS number(s): 34.80.Bm

I. INTRODUCTION

Toluene ($C_6H_5CH_3$) and benzotrifluoride ($C_6H_5CF_3$) are derived from the prototype benzene molecular structure following substitution of one of the hydrogen atoms by a methyl- and a trifluoromethyl-radical respectively. They are commonly used as solvents and as intermediaries in the production of other several organic compounds. Inhalation of toluene fumes including benzene can, however, be intoxicating and toluene is now categorized as one of the well-known chemical hazards. On the other hand, benzotrifluoride has been recognized as a more environmentally friendly organic compound [1].

In quantum chemistry, substitutions of one of the H atoms in C_6H_6 by the CH_3 and CF_3 radicals have also attracted research interest from the viewpoint of both fundamental sciences and their applications, although benzene has been investigated enormously by an infinite number of approaches. These previous studies have already been summarized in Refs. [2–4], and therefore not repeated again here. However, we report here on elastic differential-cross-section (DCS) measurements as well as theoretical studies for $C_6H_5CH_3$ and $C_6H_5CF_3$ by electron impact. The elastic channel is the most fundamental and essential in the electron molecule collision dynamics, being not only the dominant contributor to the total cross section, but also providing a guideline for theoretical testing. Furthermore, absolute elastic DCS give the benchmark cross section for the inelastic scattering ones. On C_6H_6, DCS for the electron elastic scattering have been studied experimentally by Gulley and Buckman [5], Cho *et al.* [6], and Sanches *et al.* [7], and theoretically by Gianturco and Luchesse [8] and Bettega *et al.* [9].

For the theoretical approach, although many sophisticated methods [10] have been developed by using not only analytical techniques but also computational ones for electron-molecule collisions, there is still growing awareness of the need for a fast and reliable method in a wide range of applications. From this perspective, the independent-atom method (IAM), employing a quasi-free nonempirical model, has been revised to improve its foundation and accuracy. It has successfully been tested in calculations of elastic (differential and integral) and inelastic cross sections for He, Xe, N_2, CO, and CO_2 for impact energies from 30 to a few keV [11,12].

As a part of our program for studying the substitutional effects in C-H bond-containing polyatomic molecules [13,14], a joint experimental and theoretical study has been conducted to give absolute elastic-differential and integral cross sections, and to elucidate the similarity and difference in the angular distribution between benzene and its two derivatives $C_6H_5CH_3$ and $C_6H_5CF_3$. In Secs. II and III, we briefly describe the methods employed in these measurements and theoretical procedures, respectively. In Sec. IV,

*Visiting Scientist from Ateneo de Zamboanga University, Zamboanga City, Mindanao, Philippines.
†masami-h@sophia.ac.jp
‡Visiting Scientist from Kyushu University; Present address: Atomic and Molecular Laboratories, RSPE, Australian National University, Canberra, ACT 0200, Australia.

our experimental and theoretical results are presented and compared with C_6H_6.

II. EXPERIMENTS

To measure the elastic DCS for $C_6H_5CH_3$ and $C_6H_5CF_3$ a crossed beam apparatus has been employed. A detailed description on its use and the experimental procedure is found in [15] and will therefore only be briefly summarized here. Electrons produced from an electrostatic hemispherical-monochromator intersect with an effusive molecular beam at right angles and scattered electrons are energy analyzed in a second hemispherical detector. Both the monochromator and the detector are enclosed in differentially pumped casings, to reduce the effect of background gases and to minimize the stray electric fields as well as electron background. All electron lens voltages were carefully calculated with an electron trajectories program. For some lens elements, the driving voltages were regulated by the programmable power supplies to keep the transmission of the scattered electrons constant. Overall resolution at Faraday-cup currents of 3–6 nA was about 30 meV (full width at half maximum of the observed elastic peaks), sufficient to separate the elastic peak from vibrational excitation, but not from rotational excitations. Thus in the results presented the vibrationally elastic cross sections are simply presented at part of the elastic cross sections. The incident electron energy is calibrated against the 19.36 eV resonance of He. With respect to the incident electron beam, the angular range covered is from 15° to 130°, with an angular resolution of $\pm 1.5°$.

Absolute cross sections are determined using the relative flow technique [16]. This involves the measurement of the relative electron scattering intensities for the gas under study (C_6H_6, $C_6H_5CH_3$, or $C_6H_5CF_3$) and helium (He), for which there is an accurate set of DCS. The He cross sections tabulated by Boesten and Tanaka [17] have been used. The driving pressures for both the target and reference gases are determined in such a way that their collisional mean free paths are the same in the beam-forming capillary. This is done in order to minimize the effects that collisions have on the relative shapes of the atomic and molecular beams. It is worth noting here, however, that the use of the relative flow requires knowledge of both the target and reference gas collisional diameters [15], in order to establish the correct flow rates. While these were accurately known for He and C_6H_6 from literature, they had to be estimated for $C_6H_5CH_3$ and $C_6H_5CF_3$. The estimations for these two were done based on adding the molecular constants for the known CH_4 to C_6H_6 to derive $C_6H_5CH_3$, and CF_4 to C_6H_6 to get $C_6H_5CF_3$. The results of this exercise and the subsequent driving pressures used in the relative flow technique for the current measurements are shown in Table I. Though this method for deriving the collisional diameters for $C_6H_5CH_3$ and $C_6H_5CF_3$ is rather rough, it suffices for the purpose of these experiments.

The sample gases were supplied by evaporation from the liquid phases (supplied by Wako Pure Chemical Industries Ltd., with a guaranteed purity of 99.99%) through heating. Experimental errors are estimated at 15%–20%. The experimental DCS have been measured between 1.5 and 200 eV for both $C_6H_5CH_3$ and $C_6H_5CF_3$. Note that the present data for C_6H_6 include results for higher impact energies of 50, 100, and 200 eV. Elastic integral cross sections (ECS) are determined by integration of the DCS over all of the scattering angular range of $0° \leq \theta \leq 180°$. The DCS for the inaccessible angular ranges $\theta < 15°$ and $\theta > 130°$ are obtained by an extrapolation based on elastic DCS data from the present IAM method. The overall errors arising from the present procedure are less than 30%, since the extrapolation is known to affect the minor portion of the integration.

TABLE I. Molecular collisional diameters and experimental driving pressures used in the experiments. NB. The parentheses indicate numbers that were derived and are thus not very accurate.

	He	C_6H_6	$C_6H_5CH_3$	$C_6H_5CF_3$
Diameter (Å)	2.18	7.65	(11)	(11.5)
Pressure (Torr)	3.0	0.24		
	5.0		0.2	
	5.0			0.18

III. THEORY

The present calculations of the electron molecular cross sections are based on a corrected form of the IAM known as the screen corrected additivity rule (SCAR) procedure. All the details for this procedure have been extensively described in previous works [12], where it has been applied to many other molecular species, so only a brief summary will be given here. In the standard IAM approximation, the electron-molecule collision is reduced to the problem of collision with individual atoms by assuming that each atom of the molecule scatters independently and that redistribution of atomic electrons due to the molecular binding is unimportant. At low energies, where atomic cross sections are not small compared to the interatomic distances in the molecule, the IAM approximation fails because the atoms can no longer be considered as independent scatterers and multiple scattering within the molecule is no longer negligible. These corrections have been shown to be important in many molecular systems [12]. It has been also shown that the energy range for which deviations from the IAM approximation are relevant depends on the size of the molecule: 10% or larger screening corrections take place for N_2 and CO up to 200 eV, for CO_2 up to 300 eV, and for benzene up to 600 eV. While the detailed considerations leading to the SCAR expressions are somewhat involved, the final results are relatively simple. In the first place, for integrated (elastic or inelastic) cross sections, the usual additivity rule (AR) expressions are replaced by modified ones:

$$\sigma^{elast} = \sum_i s_i \sigma_i^{elast} \quad \text{and} \quad \sigma^{inelast} = \sum_i s_i \sigma_i^{inelast}. \tag{1}$$

Here, the introduced screening coefficients $(0 \leq s_i \leq 1)$ reduce the contribution from each atom to the total cross section. Calculation of s_i coefficients requires only data on the

position and the total cross section σ_i of each atom in the molecule. The explicit expressions for s_i are [12,18]:

$$\epsilon_i^{(1)} = 1, \quad \epsilon_i^{(k)} = \frac{N-k+1}{N-1} \sum_{j(\neq i)} \sigma_j \epsilon_j^{(k-1)} / \alpha_{ij} \quad (k = 2,3,\ldots,N), \tag{2}$$

$$s_i = 1 - \frac{\epsilon_i^{(2)}}{2!} + \frac{\epsilon_i^{(3)}}{3!} - \frac{\epsilon_i^{(4)}}{4!} + \cdots \pm \frac{\epsilon_i^{(N)}}{N!}, \tag{3}$$

where N stands for the number of atoms in the molecule, the j index in sums $\Sigma_{j(\neq i)}$ runs over all the N atoms except the i one, $\alpha_{ij} = \max(4\pi r_{ij}^2, \sigma_i, \sigma_j)$, and r_{ij} is the distance between centers of atoms i and j. The successive auxiliary $\epsilon_i^{(k)}$ contributions arise from k atoms overlapping and so only $\epsilon_i^{(2)}$ exists for diatomics.

Secondly, for the elastic differential cross section, instead of the standard form

$$\frac{d\sigma^{elast}}{d\Omega} = \sum_{i,j} f_i(\theta) f_j^*(\theta) \frac{\sin qr_{ij}}{r_{ij}} = \sum_i \frac{d\sigma_i^{elast}}{d\Omega} + \sum_{i \neq j} f_i(\theta) f_j^*(\theta) \frac{\sin qr_{ij}}{r_{ij}} \tag{4}$$

(where, as usual, $q = 2K \sin \theta/2$ is the momentum transfer and $f_i(\theta)$ the scattering amplitude for the ith atom) now we have [18]

$$\frac{d\sigma^{elast}}{d\Omega} \simeq (1 - X_s) \frac{\sigma^{elast} - \sigma_D}{4\pi} + \left[1 + X_s \left(\frac{\sigma^{elast}}{\sigma_D} - 1\right)\right] \times \left(\sum_i s_i^2 \frac{d\sigma_i^{elast}}{d\Omega} + \nu \sum_{i \neq j} s_i s_j f_i(\theta) f_j^*(\theta) \frac{\sin qr_{ij}}{r_{ij}}\right), \tag{5}$$

where X_s and σ_D are defined by

$$\sigma_D = \int \frac{d\sigma_D}{d\Omega} \sin\theta d\theta = \sum_i s_i^2 \sigma_i^{elast},$$

$$X_s \approx \int_{0^\circ}^{45^\circ} \frac{d\sigma_D}{d\Omega} \sin\theta d\theta \Big/ \int_{0^\circ}^{180^\circ} \frac{d\sigma_D}{d\Omega} \sin\theta d\theta. \tag{6}$$

Expressions (5) and (6) resulted in [18] after an analysis of the angular distribution including redispersion processes inside the molecule and after some estimation on the relevance of these contributions. The normalization parameter ν (not used in [18]) is chosen so as to ensure consistency of the $d\sigma^{elast}/d\Omega$ differential values with the σ^{elast} integrated ones and affects only the positive values of $\Sigma_{i \neq j} s_i s_j f_i f_j^* \sin qr_{ij}/r_{ij}$ sum.

It must be noted that only atomic spatial coordinates are necessary for the calculation, with no consideration of the molecular symmetry or bond type, so the procedure can be easily applied to arbitrary species. Once the atomic cross sections and scattering amplitudes are known, the corrected molecular quantities are directly derived from Eqs. (1)–(3) and Eqs. (5) and (6). Screening corrections become significant only at low energies resulting in a reduction in total values and a smoothing of maxima and minima in differential cross sections.

The procedure used for calculation of the corresponding atomic cross sections has been extensively described elsewhere [11], so only a brief comment will be given here. For our purposes, the electron-atom interaction is represented by the approximate *ab initio* optical potential $V_{opt}(r) = V_s(r) + V_e(r) + V_p(r) + iV^a(r)$. Here, $V_s(r)$ is the static potential calculated by using the charge density deduced from Hartree-Fock atomic wave functions including relativistic corrections, $V_e(r)$ the exchange potential for which the semiclassical energy-dependent formula derived by Riley and Truhlar is used, $V_p(r)$ represents the target polarization potential in the form given by Zhang *et al.*, and finally the absorption potential $V^a(r)$ accounting for inelastic processes is based on the revised quasi-free model [11]. For each atom, the corresponding radial scattering equation was numerically integrated and the resulting complex partial wave phase shifts δ_ℓ were used to obtain the atomic scattering amplitudes and total cross sections [11]. In particular, the data used here for C and H atoms are exactly the same as those used in Refs. [11,18]. For each atom, the total cross section resulting from the optical theorem includes inelastic contributions arising from the $iV^a(r)$ imaginary potential, while the total elastic cross section is obtained by integrating the differential elastic values. Total inelastic cross sections are the difference between total and integrated elastic values.

For molecules with an appreciable permanent dipole moment, as is the case with $C_6H_5CF_3$, an additional contribution arising from rotational excitation should be included. This has been treated following the procedure suggested in [19]. This method consists in the calculation of the rotational excitation cross section for a free electric dipole by assuming that the energy transferred is so low, in comparison with the incident energy, to validate the first Born approximation. This contribution was added to the differential and integral values.

The average rotational excitation cross sections $J-J'$ were calculated in the first Born approximation at 300 K, by weighting with the corresponding population of J rotational quantum numbers at that temperature. In any case we have checked that temperature dependence of this contribution is negligible for this molecule

IV. RESULTS AND DISCUSSION

Figures 1(a)–1(d) and 2(a)–2(d) present elastic DCS results for $C_6H_5CH_3$ and $C_6H_5CF_3$, together with those for benzene (C_6H_6) over the energy range from 1.5 to 200 eV. The corresponding ECS and TCS for $C_6H_5CH_3$ and C_6H_6 are shown in Fig. 3. In Figs. 1 and 2 the present data are compared with the results from our previously published results for C_6H_6 at 1.1, 4.9, 8.5, 15, and 30 eV [6]. The current theoretical results are also included in both figures. We tentatively divide the molecules studied here into two groups for later discussion: (a) one for the polar molecules $C_6H_5CH_3$ (0.375 D) and $C_6H_5CF_3$ (2.86 D) [20]; and (b) another for

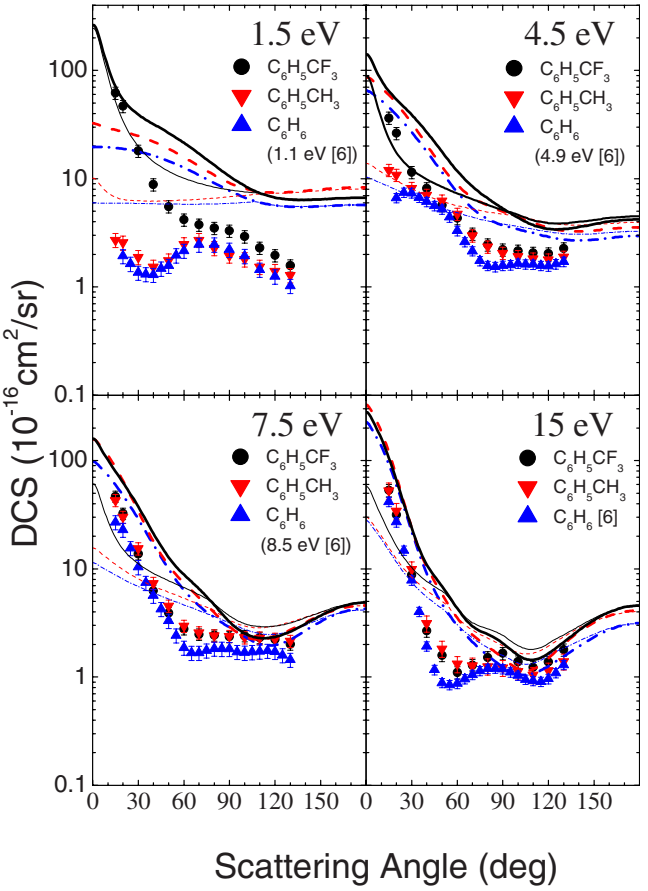

FIG. 1. (Color online) Differential elastic cross sections for $C_6H_5CH_3$ and $C_6H_5CF_3$ by electron impact at energies up to 15 eV. Lines correspond to the present theoretical elastic cross sections based on the IAM as solid for $C_6H_5CF_3$, dashed for $C_6H_5CH_3$, and dot-dashed for C_6H_6. Thin lines include the ν normalization correction while thick ones do not. The data for C_6H_6 included for comparison are from Cho *et al.* [6].

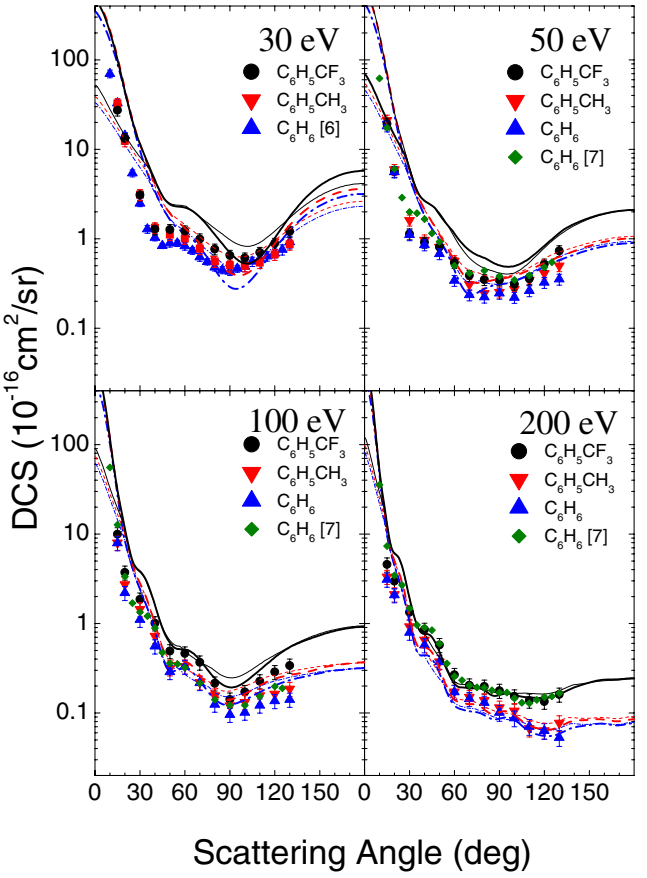

FIG. 2. (Color online) Differential elastic electron scattering cross sections for $C_6H_5CH_3$ and $C_6H_5CF_3$ for energies 30 eV and above. Solid and dashed lines represent calculated values, with notations the same as in Fig. 1. This figure includes our current results for C_6H_6 at 50, 100, and 200 eV, compared with those from literature.

the nonpolar C_6H_6. Some of the characteristic molecular constants are listed for all molecules in Table II.

A. Differential cross sections

The present results (Tables III–V) for DCS show remarkable features summarized as follows. (1) At 1.5 eV: DCS for $C_6H_5CF_3$ continue to increase steeply with decreasing scattering angles resulting in strong forward peaking at this low impact energy, a typical characteristic of a long-range dipole interaction for polar molecules like these. On the other hand, the DCS show very similar angular distributions and magnitudes for the nonpolar molecule C_6H_6 as for the polar molecule $C_6H_5CH_3$, which has a small dipole moment. However, critical analysis of these data shows that small deviations are also observed at small angles and attributable to the small dipole moment in $C_6H_5CH_3$. In addition, DCS for both C_6H_6 and $C_6H_5CH_3$ show a *d*-wave character in their angular dependencies with a maximum at 90° and a minimum at 50–60°. These reflect on the effect of the shape resonances observed in the measurements of the vibrational excitations, which revealed the π^* character enhancements in the vibra-

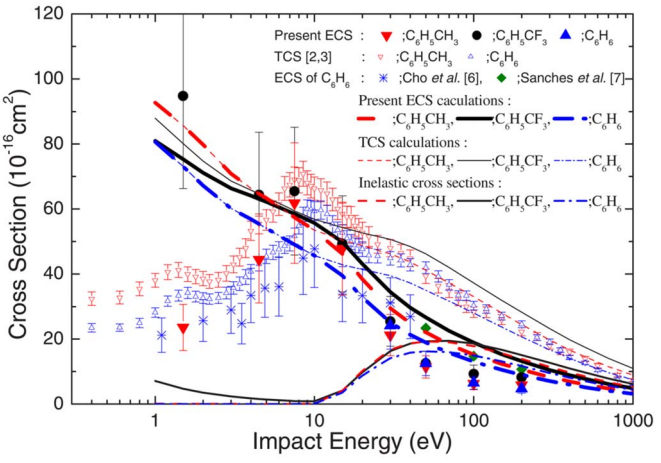

FIG. 3. (Color online) Comparison of ECS and TCS [2,3]. Lines correspond to the present theoretical ECS based on the IAM: solid for $C_6H_5CF_3$, dashed for $C_6H_5CH_3$, and dot-dashed for C_6H_6. Thin lines correspond to the elastic values while thicker ones represent the total (elastic plus inelastic) cross section.

TABLE II. Characteristic molecular constants for C_6H_5X (X =H, CH_3, and CF_3).

X	H	CH_3	CF_3
Dipole moment (μ/D)	0	0.375	2.86
Bond length (Å)			
C-C ring	1.399[a]	1.399[a]	1.40[b]
C-X		1.524[a]	1.54[b]
C-H	1.101[a]	1.11[a]	1.04[b]
C-F			1.35[b]
Polarizabilities	10.00[a]	11.80[a]	
(10^{-24} cm^3)	10.32[a]	12.26[a]	None
	10.74[a]	12.30[a]	
Symmetry	D_{6h}	C_8	C_8

[a]Reference [20]; for the polarizability, three kinds of values are shown in Ref. [20].
[b]Reference [21].

tional excitation at 1.1 eV [6]. It is also worth noting that near-complete overlap is observed for the DCS for $C_6H_5CH_3$ and C_6H_6. (2) At 4.5 eV: the forward peaking trend is still visible in the DCS for $C_6H_5CF_3$, while the minima for both $C_6H_5CH_3$ and C_6H_6 are growing to emerge as broad shoulders around 60°. From 70° to 130° these three DCS show isotropic angular distribution. Salient features in the present results are clearly apparent in that all the three DCS curves resemble each other. (3) At the higher impact energies 15–50 eV, more undulations can be seen due to the higher partial waves involved in the scattering dynamics. Below 50°, the sharp forward peaking in DCS is very similar and a common feature to all molecules, indicating the lesser significance of the dipole interaction at these energies. (4) At 100 and 200 eV, new bumps and dips begin to appear clearly at forward scattering angles, which is ascribable to the interference from multicenter scattering in the molecules. It should also be noted that the magnitudes of the DCS for $C_6H_5CF_3$ are slightly larger than those for $C_6H_5CH_3$ and C_6H_6 over the scattering angles measured. (5) The present DCS for C_6H_6 at 50, 100, and 200 eV are in good agreement with the recent experimental results of Sanches *et al.* [7] within the experimental uncertainties. (6) Exclusive of the dipole moment in $C_6H_5CF_3$ below 4.5 eV, it is clear from these data that the signature of the benzene ring is predominant in the scattering dynamics for all three molecules.

TABLE III. Absolute DCS (in units of 10^{-16} cm^2 sr^{-1}) for elastic electron scattering from C_6H_6. The uncertainties are estimated to be 15%–20%. Q_i and Q_m are the ECS and momentum transfer cross sections in units of 10^{-16} cm^2 sr^{-1}, respectively.

θ (deg)	Impact energy (eV) 50	100	200
15	18.200	7.929	3.100
20	5.565	2.197	2.076
30	1.105	1.102	0.793
40	0.852	0.556	0.572
50	0.678	0.287	0.371
60	0.341	0.329	0.171
70	0.235	0.217	0.144
80	0.222	0.124	0.130
90	0.245	0.095	0.101
100	0.220	0.101	0.087
110	0.262	0.121	0.070
120	0.324	0.136	0.063
130	0.352	0.141	0.053
Q_i	12.53	6.52	4.74
Q_m	4.66	2.14	1.35

B. Comparison between ECS and TCS

Detailed comparison between the ECS and the TCS is shown in Fig. 3 for $C_6H_5CH_3$ and C_6H_6. For $C_6H_5CF_3$, however, we compare the experimental ECS with the IAM theoretical ECS. Experimental ECS are obtained by integration of the present DCS over the measured scattering angular range of θ, with extrapolation of the DCS to the regions $0° \leq \theta \leq 15°$ and $130° \leq \theta \leq 180°$ done based on the IAM. The TCS for $C_6H_5CH_3$ shown here have been discussed elsewhere [3] and will be described briefly here for comparison with the elastic ECS. (1) The TCS for $C_6H_5CH_3$ and C_6H_6 show a strong hump commonly around 7–10 eV, a rapid decreasing trend with increasing impact energy, and a discontinuity observed as a broad shoulder around 20–40 eV. The magnitudes of these TCS are nearly equal above 30 eV, i.e., a phenomenon also observed for the ECS of all three molecules within the error bars. (2) Below 20 eV, the TCS for $C_6H_5CH_3$, however, are slightly larger than those for C_6H_6, which is qualitatively consistent with the trend observed in the present ECS results, in the limit of the experimental errors. (3) At the lower energy sides with respect to the peak, these TCS share two common visible structures: the sharper peak at 1.5 and a broad shoulder around 4 eV. These structures are attributed to the shape resonances arising from the temporary trapping of the electron into the antibonding orbitals. They were observed in the C-H stretching vibrational excitation modes, 1.4, 5, and 7.5 eV for $C_6H_5CH_3$ and 1.4, 5, and 8 eV for C_6H_6, i.e., in agreement with the energy dependence in the corresponding TCS. Similar resonance features have also been observed at 4 and 7 eV for $C_6H_5CF_3$ [4]. It is worth noting too that in contrast to the decreasing trend observed in both the TCS and ECS for these two molecules, the ECS for $C_6H_5CF_3$ show a rather rapidly rising trend, in the limit of the errors due to the extrapolation based on the current IAM DCS. However, this rising trend with decreasing energy is rather expected due to the dipole induced long-range scattering for these polar $C_6H_5CF_3$ molecules.

C. Comparison between experimental and theoretical results

In order to obtain a better understanding of the observed features, we carried out a theoretical study using the IAM. In

TABLE IV. Absolute DCS (in units of 10^{-16} cm^2 sr^{-1}) for elastic electron scattering from $C_6H_5CH_3$. The uncertainties are estimated to be 15%–20%. Q_i and Q_m are the ECS and momentum transfer cross sections in units of 10^{-16} cm^2 sr^{-1}, respectively.

θ	Impact energy (eV)							
(deg)	1.5	4.5	7.5	15	30	50	100	200
15	2.72118	12.01507	42.93319	52.896	32.566	21.127	8.017	3.333
20	2.571	10.856	30.049	34.301	12.398	5.950	2.736	2.119
30	1.887	8.201	15.429	9.895	3.106	1.611	1.444	0.926
40	1.542	7.066	7.368	3.135	1.325	0.969	0.726	0.656
50	1.763	6.247	4.553	1.832	1.110	0.811	0.315	0.376
60	2.490	4.718	2.970	1.324	1.008	0.567	0.331	0.173
70	2.721	2.979	2.571	1.278	0.773	0.308	0.220	0.151
80	2.291	2.362	2.418	1.254	0.557	0.246	0.157	0.139
90	1.952	2.057	2.383	1.221	0.505	0.253	0.121	0.115
100	1.800	1.917	2.328	1.132	0.497	0.273	0.132	0.106
110	1.534	1.825	2.305	1.048	0.541	0.346	0.156	0.067
120	1.410	1.789	2.254	1.150	0.667	0.411	0.163	0.064
130	1.285	1.897	2.161	1.395	0.867	0.498	0.186	0.077
Q_i	23.55	44.47	61.81	47.80	21.18	11.43	6.28	5.79
Q_m	21.28	28.85	34.69	19.94	11.51	5.87	2.58	1.52

general, the result of the comparison between the calculation and the experimental values is similar to that previously observed for other molecular targets [18]. At intermediate and higher energies (above 50 eV) good agreement is observed both for the elastic DCS and the theoretical ECS. Over the energy range 10–50 eV there is reasonable agreement between the theoretical and experimental ECS, although discrepancies appear at small scattering angles for the DCS. Above 50 eV, reasonable qualitative and quantitative agreement is observed between the measured TCS and the IAM TCS, i.e., derived as the sums of the IAM ECS and inelastic cross sections shown in Fig. 3. Finally, below 10 eV, the

TABLE V. Absolute DCS (in units of 10^{-16} cm^2 sr^{-1}) for elastic electron scattering from $C_6H_5CF_3$. The uncertainties are estimated to be 15%–20%. Q_i and Q_m are the ECS and momentum transfer cross sections in units of 10^{-16} cm^2 sr^{-1}, respectively.

θ	Impact energy (eV)							
(deg)	1.5	4.5	7.5	15	30	50	100	200
15	61.801	36.349	46.608	53.091	27.359	19.222	9.968	4.576
20	46.725	26.278	32.430	31.600	13.185	5.657	3.716	2.968
30	18.073	11.465	13.711	8.768	3.084	1.133	1.860	1.335
40	8.823	8.125	6.282	2.680	1.281	0.911	1.007	0.855
50	5.527	5.692	3.904	1.592	1.265	0.807	0.492	0.575
60	4.186	4.319	2.780	1.102	1.219	0.541	0.463	0.267
70	3.747	3.097	2.480	1.288	0.993	0.388	0.367	0.204
80	3.505	2.465	2.442	1.517	0.765	0.348	0.214	0.198
90	3.301	2.209	2.366	1.658	0.651	0.345	0.141	0.177
100	2.928	2.161	2.404	1.385	0.608	0.310	0.172	0.153
110	2.300	2.064	2.320	1.232	0.704	0.357	0.226	0.138
120	1.954	2.037	2.229	1.383	0.887	0.520	0.287	0.134
130	1.573	2.268	2.005	1.790	1.206	0.731	0.339	0.161
Q_i	94.74	64.33	65.46	49.29	25.46	12.50	9.24	8.24
Q_m	35.32	32.98	33.89	23.40	16.07	8.21	4.48	2.62

present approximation is no longer valid and it is not able to justify either the integrated experimental values or the resonance effects. In this energy region the used approximation also fails for the DCS values, and only the dipole contribution seems to be correctly justified.

V. CONCLUSION

Absolute DCS for elastic scattering from two benzene derivatives $C_6H_5CH_3$ and $C_6H_5CF_3$ have been measured for the scattering angles of $15°-130°$ and at impact energies 1.5–200 eV. Both DCS are compared to those of C_6H_6. The present experimental results show that (1) the three molecules have very similar magnitudes and shapes of the DCS at 7.5–200 eV; (2) the DCS for $C_6H_5CF_3$ increase steeply toward lower scattering angles due to the dipole moment at 1.5 and 4.5 eV; (3) at 1.5 eV, DCS for both $C_6H_5CH_3$ and $C_6H_5CF_3$ confirm the evidence of a *d*-wave resonant angular character observed in the vibrational excitation; and (4) the molecular structure of the benzene ring dominates overall features in those collision dynamics. Furthermore, by employing the IAM, within the quasi-free nonempirical model, DCS calculations have been carried out independently without any empirical parameter fittings, i.e., in an *ab initio* nature. The calculated DCS are in excellent agreement with the experimental values at 30, 50, 100, and 200 eV. It is concluded that an approximate *ab initio* model known as the quasi-free absorption model is verified to be a useful technique of reasonable accuracy and simplicity in studying electron scattering for a broad range of polyatomic molecules.

ACKNOWLEDGMENTS

This work was supported in part by a Grant-in-Aid from the Ministry of Education, Science, Technology, Sport and Culture, Japan, the Japan Society for the Promotion of Science (JSPS) through Sophia University, and a Cooperative Research Grant from the National Institute for Fusion Science (NIFS). This work was also performed under the IAEA Coordinated Research Program on Atomic and Molecular Data for Plasma Modeling. H.K. gratefully acknowledges the JSPS for financial support. M.C.G. is also grateful to Sophia University for financial support. F.B. and G.G. were also supported by the Spanish Ministerio de Ciencia e Innovación (Project No. FIS0032-00702) and the European Science Foundation (EIPAM network and COST Action CM0601).

[1] J. J. Maul, P. J. Ostrowski, G. A. Ublacker, B. Linclau, and D. P. Curran, *Modern Solvents in Organic Synthesis*, edited by P. Knochel (Springer-Verlag, Berlin, 1999), p. 206.
[2] C. Makochekanwa, O. Sueoka, and M. Kimura, Phys. Rev. A **68**, 032707 (2003).
[3] H. Kato, C. Makochekanwa, Y. Shiroyama, M. Hoshino, N. Shinohara, O. Sueoka, M. Kimura, and H. Tanaka, Phys. Rev. A **75**, 062705 (2007).
[4] H. Kato, S. Kobayashi, C. Makochekanwa, M. Hoshino, N. Shinohara, O. Sueoka, H. Cho, and H. Tanaka, Phys. Rev. A **79**, 062702 (2009).
[5] R. J. Gulley and S. J. Buckman, J. Phys. B **32**, L405 (1999).
[6] H. Cho, R. J. Gulley, K. Sunohara, M. Kitajima, L. J. Uhlmann, H. Tanaka, and S. J. Buckmann, J. Phys. B **34**, 1019 (2001).
[7] I. P. Sanches, R. T. Sugohara, L. Rosani, M.-T. Lee, and I. Iga, J. Phys. B **41**, 185202 (2008).
[8] F. A. Gianturco and R. R. Lucchese, J. Chem. Phys. **108**, 6144 (1998).
[9] M. H. F. Bettega, C. Winstead, and V. McKoy, J. Chem. Phys. **112**, 8806 (2000).
[10] *Computational Methods for Electron-Molecule Collisions*, edited by F. A. Gianturco and W. M. Huo (Plenum Press, New York, 1995).
[11] F. Blanco and G. Garcia, Phys. Rev. A **67**, 022701 (2003).
[12] F. Blanco and G. Garcia, Phys. Lett. A **317**, 458 (2003); **330**, 230 (2004).
[13] H. Tanaka, T. Masai, M. Kimura, T. Nishimura, and Y. Itikawa, Phys. Rev. A **56**, R3338 (1997).
[14] M. Hoshino, H. Kato, C. Makochekanwa, S. J. Buckman, M. J. Brunger, H. Cho, M. Kimura, D. Kato, I. Murakami, T. Kato, and H. Tanaka, *NIFS Data* (National Institute for Fusion Science, Toki, 2008), Vol. 101.
[15] H. Tanaka, T. Ishikawa, T. Masai, T. Sagara, L. Boesten, M. Takekawa, Y. Itikawa, and M. Kimura, Phys. Rev. A **57**, 1798 (1998).
[16] S. K. Srivastava, A. Chutjian, and S. Trajmar, J. Chem. Phys. **63**, 2659 (1975).
[17] L. Boesten and H. Tanaka, At. Data Nucl. Data Tables **52**, 25 (1992).
[18] F. Blanco and G. Garcia, Phys. Lett. A **360**, 707 (2007).
[19] A. Jain, J. Phys. B **21**, 905 (1988).
[20] *CRC Handbook of Chemistry and Physics*, edited by D. R. Lide, 81th ed. (CRC Press, New York, 2000).
[21] N. A. Narasimham, J. R. Nielsen, and R. Theimer, J. Chem. Phys. **27**, 740 (1957).